https://doi.org/10.5194/egusphere-2024-3177
Preprint. Discussion started: 28 October 2024

Effects of sudden stratospheric warmings on the global ionospheric total electron content using a machine learning analysis

Guanyi Ma[1], Klemens Hocke[2,3]

[1]National Astronomical Observatories, Chinese Academy of Sciences, Beijing 100101, China

[2]Institute of Applied Physics, University of Bern, 3012 Bern, Switzerland

[3]Oeschger Centre for Climate Change Research, University of Bern, 3012 Bern, Switzerland

Correspondence to: Guanyi Ma (guanyima@nao.cas.cn), Klemens Hocke (klemens.hocke@unibe.ch)

Abstract. A sudden stratospheric warming is a breakdown of winter stratospheric polar vortex. It has atmospheric effects in both the Northern and Southern hemispheres, leading to disturbances in the whole ionosphere. Previous works with case studies have shown that SSW effect is mainly in low-latitude ionosphere and each SSW event may have a different effect on the ionosphere due to complex dynamics from solar/geomagnetic activities and seasonal changes. However, the SSW induced tidal variability in mid to high-latitude ionosphere is only identified for several events and its behaviour is not well understood. Here we analyze SSWs' influences on diurnal/semidiurnal variations of global ionosphere with the global maps of total electron content (TEC) from 1998 to 2022. We use machine learning (ML) with neural network to establish the TEC (ML-TEC) model related to the solar/geomagnetic activities and seasonal change from the long-term global TEC data. The TEC variations due to SSWs are extracted by subtracting the ML-TEC from the observed TEC. Comprehensive composite analysis of 18 SSW events shows for the first time a globally SSW-induced enhancement in diurnal/semidiurnal TEC variations. The enhancement is the strongest at equatorial ionospheric anomaly (EIA) crests, moderate in mid-latitude and vague in high-latitude ionosphere. It also exhibits hemispheric asymmetry and longitudinal differences. While the semidiurnal enhancement starts earlier and peaks at ~8 days after SSW onset, the diurnal one starts on the SSW onset day and peaks around 20-30 days after SSW onset. The enhancement of both semidiurnal and diurnal TEC variations lasts to

https://doi.org/10.5194/egusphere-2024-3177
Preprint. Discussion started: 28 October 2024

about 50 days after SSW onset. The SSW related E-region dynamo is likely the dominant mechanism which is not strong enough to produce discernible TEC variations in high-latitude ionosphere. ML-TEC does not contain the SSW effect and is thus a valuable reference for the ionospheric state without an SSW.

1 Introduction

A sudden stratospheric warming event is associated with a breakdown and reversal of the stratospheric polar vortex of the winter hemisphere. This severe disturbance of the vortex is caused by the interaction of upward propagating planetary waves and the stratospheric zonal mean wind during the winter months. SSWs are the most spectacular manifestation of vertical coupling between different atmospheric layers. They also have great atmospheric effects in the hemisphere opposite from the location of the original SSW, causing changes in the whole atmosphere and ionosphere (Pedatella et al., 2018).

The underlying mechanism can be modified E-region dynamo for ionosheric effects observed at low to mid-latitudes. It is assumed that an SSW induces a change of the mesospheric polar vortex. The upward propagating atmospheric tides from below are often amplified in the modified mesospheric wind field and induce stronger electric field variations in the ionospheric dynamo region during an SSW. The electric field variations at low and middle latitudes are mapped via the magnetic field lines into the low latitude F region where E x B plasma drifts lead to considerable changes of the equatorial plasma distribution during an SSW (Jin et al., 2012; Pedatella and Liu, 2013; Pedatella et al., 2014). Ionospheric variations at mid-latitude are also explained by changes in F-region thermospheric wind, combination of tidal disturbances in thermospheric wind and electric field, and upwelling in changed O/N_2 thermospheric composition caused by upward-propagating solar/lunar tidal amplifications due to SSW effects on the middle atmosphere (Fuller-Rowell et al.,2010; Chernigovskaya et al., 2018; Goncharenko et al., 2021).

https://doi.org/10.5194/egusphere-2024-3177
Preprint. Discussion started: 28 October 2024

The majority of previous works conducted case studies to analyze the impacts of the SSW on the ionosphere. There are indications that each SSW event may have a different effect on the ionosphere due to complex dynamics from solar and geomagnetic activities (Goncharenko et al., 2021). Moreover, the effect is particularly large in the low-latitude, where a strongly amplified semidiurnal pattern in the vertical ion drift, equatorial electrojet and TEC have been observed (Chau et al., 2009; Yamazaki et al., 2012; Goncharenko et al., 2021). SSW induced tidal variability in mid-latitude ionosphere are only identified for a few events although enhancement in F-region electron density, height and temperature have been observed (Xiong et al., 2013; Chen et al., 2016; Goncharenko et al., 2018; Liu et al., 2019). In high-latitude ionosphere the discerned response to SSW is confined to decrease of peak electron density and cooling/warming of ion temperature (Kurihara et al., 2010; Yasyukevich, 2018).

There has been a lack of statistical analysis on ionospheric effects related to SSWs. The average behaviour of the SSW-induced ionospheric changes is not well understood. Recently a composite analysis of 29 major SSW events was performed with the long-term series of peak electron density (NmF_2) over Okinawa in the northern border of the low-latitude ionosphere. Moderate SSW influence was found in the semidiurnal amplitude averaged across 29 major SSW events compared with that in the no-SSW years (Hocke et al., 2024a). However, the general effects of SSW on the tidal variability in the mid to high-latitude ionosphere has never been addressed from a statistical perspective.

This paper uses the long-term time series of global TEC to derive an average tidal/semidiurnal response of the global ionosphere to major SSWs by means of a comprehensive composite analysis. The diagnosis of the SSW effect becomes relatively straightforward since the accidental ionospheric variations during SSW events can be smoothed out. On the other

https://doi.org/10.5194/egusphere-2024-3177
Preprint. Discussion started: 28 October 2024

hand it is crucial to quantify ionospheric disturbances driven by SSWs from the atmosphere below and to distinguish those disturbances from solar/geomagnetic forcing above. Moreover, the seasonal change should be separated from the SSW effect. We use machine learning (ML) with neural network to extract the TEC (ML-TEC) series or model related to the solar/geomagnetic activities and seasonal change from the long-term TEC data. Then the TEC variations due to SSWs and atmospheric forcing from below can be obtained by subtracting the ML-TEC from the observation. The data and methodology are described in Section 2. Presented in Section 3 are the results of data analysis. Discussion is in Section 4 and conclusions are given in Section 5.

2 Data and Methodology

The ionospheric vertical TEC (just referred to as TEC in this paper) can be derived by using the dual-frequency measurements from Global Navigation Satellite System (GNSS) ground receivers due to the dispersive characteristics of the ionosphere. With the worldwide GNSS network, the International GNSS Service (IGS) has routinely provided global ionospheric maps (GIMs) of TEC (GIM-TEC) with a time resolution of 2 h and a spatial resolution of 5° in longitude and 2.5° in latitude since 1998. The map has 71x73 grid points in latitude and longitude. Details on the derivation and evaluation of the GIM-TEC were described by Hernández‑Pajares et al. (2009). Accumulated more than two solar cycles, the long term dataset of global TEC has been used for construction of ionospheric TEC model, analysis of climatological characteristics of the ionosphere and space weather. Recently IGS GIMs have been used to study lunar tides in the ionosphere (Pedatella, 2014; Hocke et al., 2024b). The GIM-TEC used in this paper is from 1998 through 2022.

There are 18 major SSW events from 1998 to 2022 and all of them happened in the Northern hemispheric winter. Table 1 presents the SSWs in their central date, which is also referred to as onset day of SSW hereafter.

https://doi.org/10.5194/egusphere-2024-3177
Preprint. Discussion started: 28 October 2024

Table 1. Central dates of the 18 SSW events from 1998 to 2022 in the Northern hemisphere.

19981215	19990225	20010211	20011230	20020217	20030118	20040105	20060120	20070224
20080222	20090124	20100209	20100323	20130106	20180211	20190101	20210104	20220322

The primary factor that determines the TEC is solar extreme ultraviolet radiation. The solar radio flux at 10.7 cm (F10.7) and Lyman-alpha (Lα) are generally used as proxies for the solar activity. Deviations of the ionosphere from its background can be caused by geomagnetic disturbances. Kp index is a globally averaged indicator of the worldwide level of geomagnetic activity. Day of year informs about the seasonal change in the atmosphere. These four kinds of data are used as driven parameters to quantify the TEC variations associated with solar, magnetospheric and seasonal variations. We use machine learning with a multilayer feed-forward neural network (MFFNN) to construct the ML-TEC model from the GIM-TEC. The MFFNN consists of the input layer, two hidden layers and the output layer. A schematic diagram of data flow in the network is shown in figure 1. The input layer has 8 nodes. F10.7 and Lα for solar activity, Kp for geomagnetic activity, Kp(-3 d) for 3-day delayed geomagnetic activity, $cos(2\pi \frac{h}{24})$ and $sin(2\pi \frac{h}{24})$ represent the diurnal variation in ionospheric TEC due to the earth rotation and revolution, $cos(2\pi \frac{DOY}{365})$ and $sin(2\pi \frac{DOY}{365})$ associate with the seasonal variation in ionospheric TEC. The number of nodes in each hidden layers is 30. The output layer is the modeled TEC (TEC_m) from the neural network. The network is trained by backpropagation by using an approximate steepest decent rule to minimize the squared residual error of the TEC_m and fine-tune the weights (Hagan and Menhaj, 1994). We consequently obtain the ML-TEC model determined by the solar/geomagnetic activities and seasonal change.

https://doi.org/10.5194/egusphere-2024-3177
Preprint. Discussion started: 28 October 2024

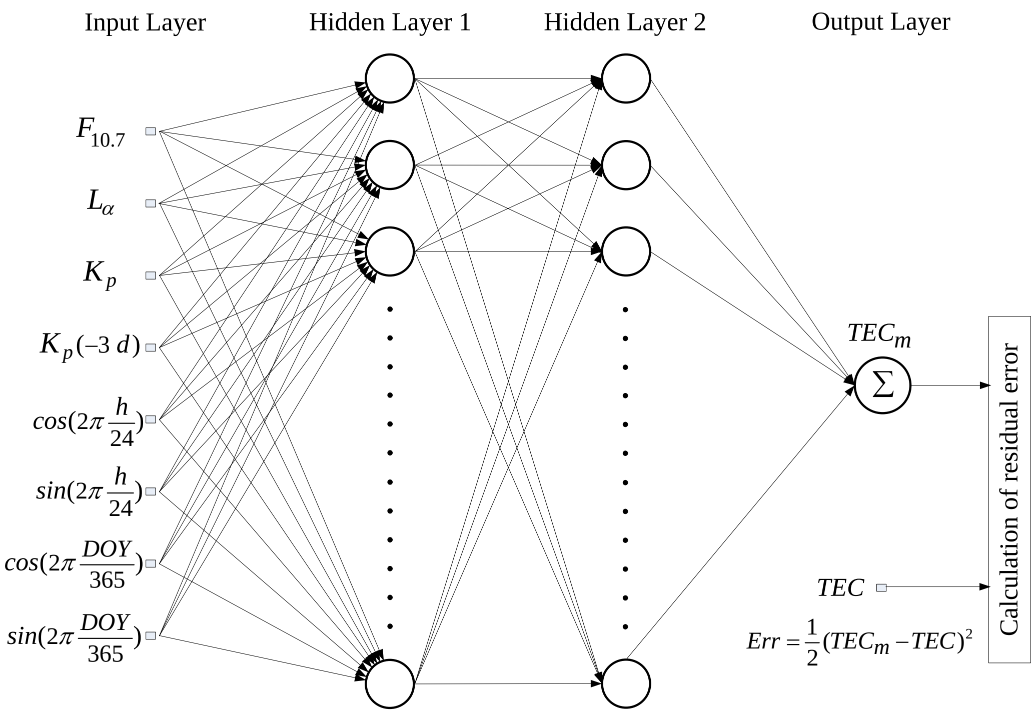

Figure 1. Schematic diagram of the MFFNN for modeling ionospheric TEC in association with solar/geomagnetic activities and seasonal change.

The diurnal (s_1) and semidiurnal (s_2) components in TEC time series are obtained with a digital non-recursive, finite-impulse-response (FIR) filter. It performs zero-phase filtering by processing the time series in forward and reverse directions which helps preserve features in a filtered time waveform exactly where they occur in the unfiltered signal. For band-pass filtering, the cutoff frequencies are at $f_c = f_p \pm 10\% f_p$, where f_c is the cutoff frequency and f_p fp is the central frequency. For the diurnal and semidiurnal variations, the cutoff frequencies are 0.9/1.1 and 1.8/2.2 cycles per day (cpd), respectively (Hocke et al., 2024; Studer et al., 2012).

https://doi.org/10.5194/egusphere-2024-3177
Preprint. Discussion started: 28 October 2024

For the 18 SSW events listed in Table 1, by using the time series of TEC with 2 h resolution, 18 subsets of the observed and modeled global TECs are created that started 200 days before the central date of SSW and ended 200 days after. The flowchart of the further data processing is shown in figure 2. For each SSW event, s_1 / s_2 of both the observed and modeled TECs are extracted by applying the FIR filter to the corresponding dataset. They are referred to as s_{1o}, s_{2o}, s_{1m} and s_{2m}, respectively. With diurnal and semidiurnal components of 18 SSW events, the composite analysis calculates the mean of S_1 / S_2 for the observed and modeled TECs, represented as S_{1o}, S_{2o}, S_{1m} and S_{2m}, respectively. It can be expected that an inherent effect of SSW can be seen well in the mean values while accidental variations contributed to S_1 and S_2 compensate one another. Then the difference of the composites between observation and model is taken, expressed as ΔS_1 and ΔS_2. This operation removed the solar/geomagnetic and seasonal effects in the diurnal and semidiurnal components and only those driven by the atmosphere below are remained.

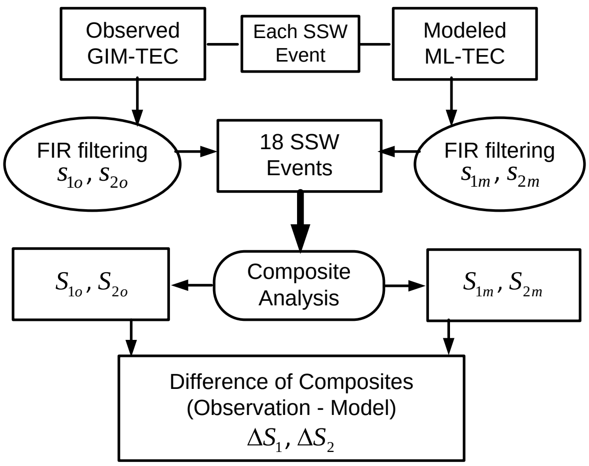

Figure 2. Flowchart of FIR filtering of GIM TEC and ML-TEC, and composite analysis of tidal TEC variations for the 18 SSWs.

https://doi.org/10.5194/egusphere-2024-3177
Preprint. Discussion started: 28 October 2024

3 Results

We begin with a case study for the major SSW event of 25 February 1999 as shown in figure 3. The top panel presents the diurnal components at grid point (30°N, 105°E) for both the observed GIM-TEC (black line) and modeled ML-TEC (red line). The middle panel is for the semidiurnal components at grid point (30°N, 80°E). The bottom panel gives F10.7 and Kp indices to show the solar and geomagnetic conditions during the event. The epoch time is from 50 days before the onset of SSW and 100 days after the onset of SSW. The two s_1 time series start to increase around SSW onset although they are close to each other and oscillate together in the preceding time. However, the s_1 of the observed TEC shows a maximum at an epoch time of 20 days, which is ~5.0 TECU larger than the modeled one. The s_1 of the observed TEC keeps larger than that of the ML-TEC for about ~50 days. The s_2 of the observed TEC also oscillate together with that of modeled TEC, and has a maximum at 20 days. The largest difference is ~3.6 TECU between the observed and modeled ones. The SSW effect on s_2 keeps for about 80 days. Both s_1 and s_2 from the modeled TEC correlate with F10.7 variation while there is no obvious variation corresponding to geomagnetic activities.

https://doi.org/10.5194/egusphere-2024-3177
Preprint. Discussion started: 28 October 2024

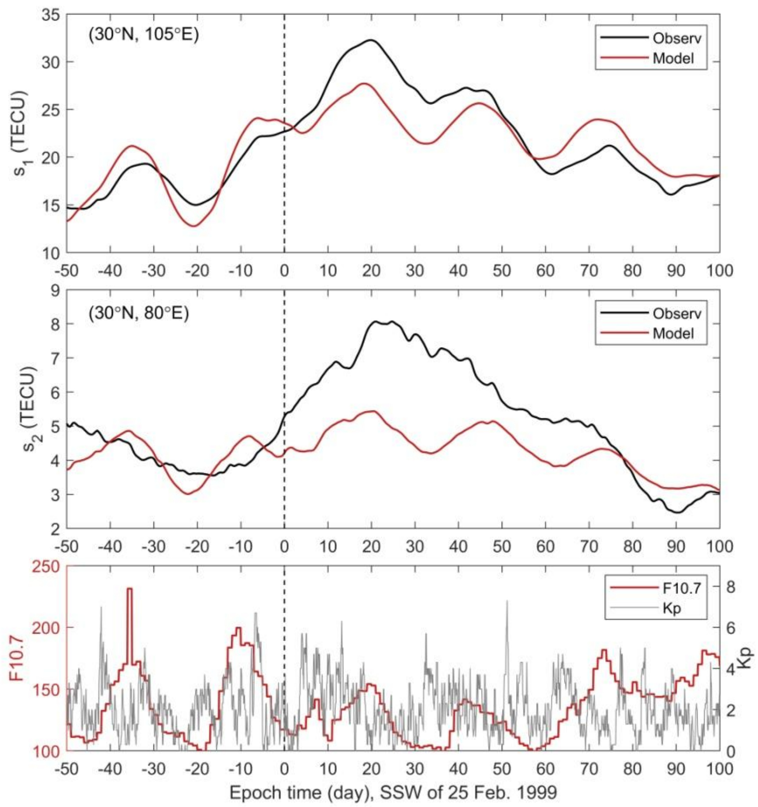

Figure 3. Diurnal TEC variation at (30 °N, 105 °E) (top panel) and semidiurnal variation at (30 °N, 85 °E) (middle panel) from observed TEC (black lines) during a major SSW event centered on 25 Feb. 1999 (marked as the vertical grey lines). Together shown are the diurnal and semidiurnal components from modeled TEC (red lines) for the event. The solar and geomagnetic conditions during the event are displayed by F10.7 (red line) and Kp (grey line) (bottom panel).

Figure 4 exhibits world maps of ΔS_1 from composite analysis of the 18 SSW events, (a) is global Delta S1 at 13 days before SSW onset and (b) is that at 25 days after SSW onset. The thick black line in each map depicts the magnetic equator. Obviously, geomagnetic electric field influences the ionospheric diurnal variation. At 13 days before SSW onset, positive ΔS_1 is seen mainly in a narrow band along magnetic equator in Asia and Pacific Ocean, northern America, and southern

https://doi.org/10.5194/egusphere-2024-3177
Preprint. Discussion started: 28 October 2024

EIA in African sector. Conspicuous negative ΔS_1 locates at EIA in Northern hemisphere and extends to all longitudes along the magnetic equator. In southern hemisphere, negative ΔS_1 takes place in most area except the bottom of southern America. At 25 days after SSW onset, an enhancement of ΔS_1 can be seen globally although it is not significant at low to mid-latitudes over Pacific, Atlantic and Indian oceans in southern hemisphere. The largest ΔS_1 enhancement is 2.25 TECU and locates at (2.5 °S, 90 °W). For the enhancement larger than 2 TECU, they distributed in a latitude range of [2.5 °S, 25 °N] and a longitude range of [155 °W, 120 °E]. An enhancement of 0.5 TECU can happen at 70 °N. In southern atmosphere, the enhancement can reach to 0.9 TECU at Antarctic. Largest ΔS_1 is ~1.95 TECU and locates at 2.5N and [45 °W, 50 °W]. For ΔS_1 lager than 1.8, they distribute at [0, 5N] and [95 °W, 40 °W], and [22.5 °N 35 °E] along the magnetic equator. It can generally reach to 32 °N. In America sector ΔS_1 shows conspicuous SSW effects from low to high latitudes.

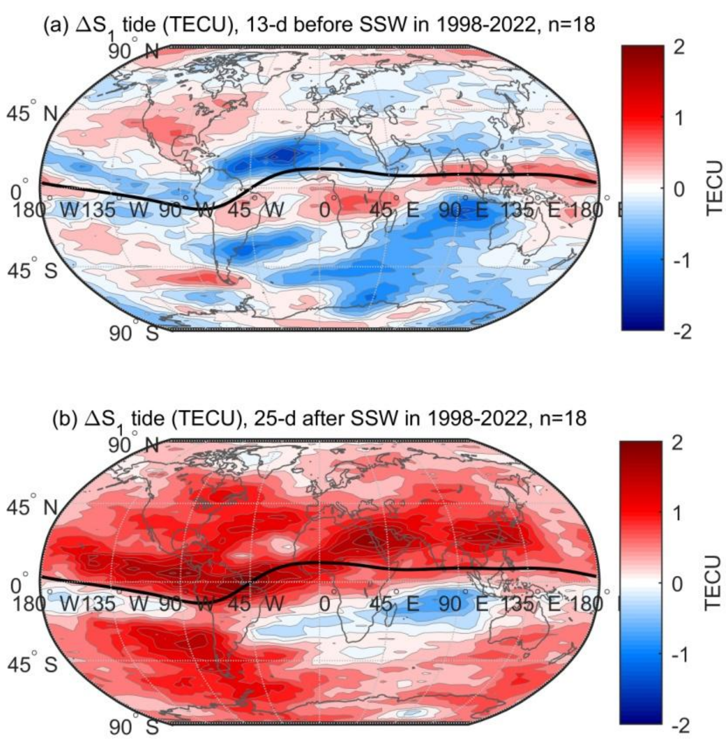

https://doi.org/10.5194/egusphere-2024-3177
Preprint. Discussion started: 28 October 2024

Figure 4. Distribution of ΔS_1 from composite analysis of the 18 SSW events. (a) global ΔS_1 at 13 days before SSW onset and (b) global ΔS_1 at 25 days after SSW onset. The thick black line in each map depicts the magnetic equator.

The global distributions of semidiurnal TEC variation are shown in figure 5. At 12 days before SSW onset in the Northern hemisphere, ΔS_2 driven by the atmosphere below is generally between 0 and 0.5 TECU in magnitude. They are manifested as patches at low latitudes along the magnetic equator, although a few larger patches can be seen at mid and high latitudes. In the Southern hemisphere ΔS_2 is more active. Large patches or belts fill at low to mid-latitudes and high latitude. The largest value is ~0.9 TECU at (40 °S, 80 °W) and (15 °S, 5 °W). At 8 days after SSW onset we can see ΔS_2 is globally enhanced except Russia, east Europe, central of North America and Pacific Ocean at ~45 °N. In the Southern hemisphere only several white patches can be seen with much smaller areas. The largest enhancement is ~1.85 TECU at ~20 °S in Pacific Ocean. ΔS_2 peaks along the magnetic equator at EIA in both hemispheres with the largest value of ~2.2 TECU.

https://doi.org/10.5194/egusphere-2024-3177
Preprint. Discussion started: 28 October 2024

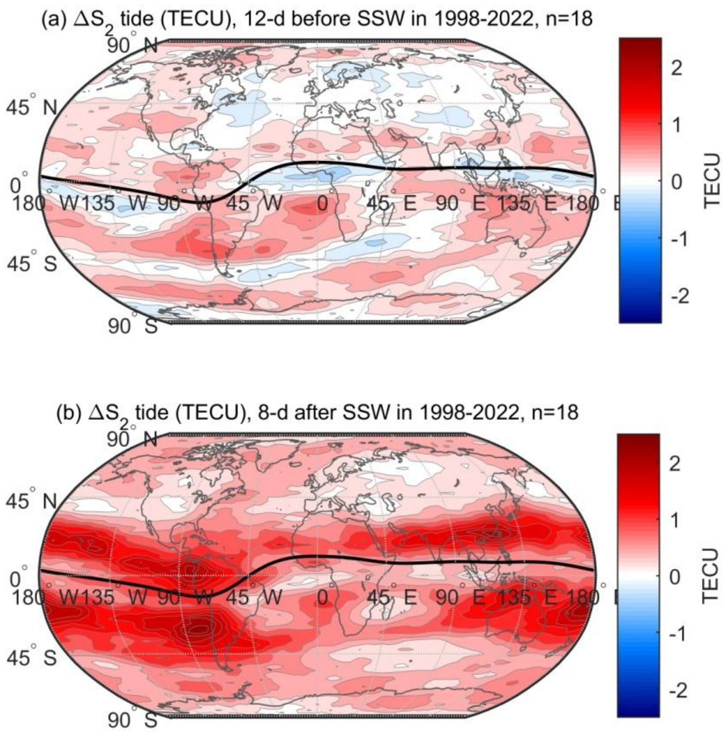

Figure 5. Distribution of ΔS_2 at 12 days before SSW onset (a) and 8 days after SSW onset (b). The thick black line in each map depicts the magnetic equator.

It is also worthwhile to examine the ionospheric tidal variabilities over time. Figure 6 shows the time variation of ΔS_1 at 90 °E, which is smoothed as a 14 d average. An enhancement of ΔS_1 can be seen from the SSW onset to ~35 days after the SSW onset in the whole northern latitudes. From ~5 °N to ~60 °N the prominent positive ΔS_1 starts to appear simultaneously at the onset day of SSW and ends at ~40 days. The strongest enhancement happens from ~5 to ~35 °N. At ~30 °N, Delta1 shows a peak level of ~1.4 TECU around 25 days. At ~15 °N, ΔS_1 maintains the highest level from ~10 to ~35 days after the SSW onset. Note that there is no systematic enhancement during the entire SSW at 90 °E in Southern hemisphere.

https://doi.org/10.5194/egusphere-2024-3177
Preprint. Discussion started: 28 October 2024

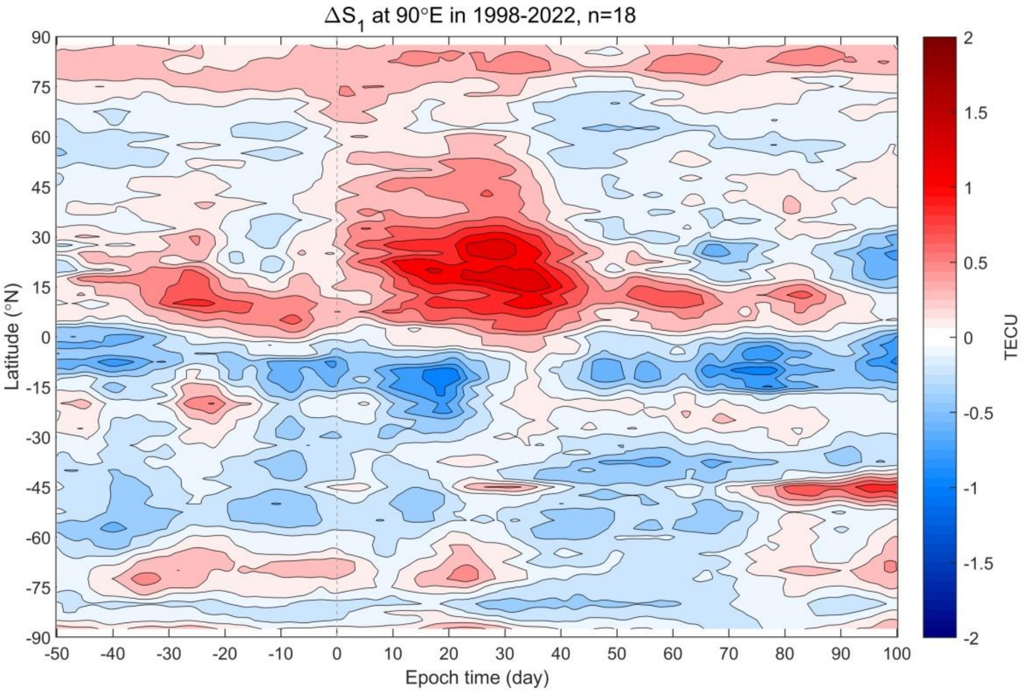

Figure 6. Time variation of meridian ΔS_1 at 90 °E, which is smoothed as a 14 d moving average. The vertical grey line marks the SSW onset day.

Figure 7 is the meridian plot of smoothed ΔS_2 at -80 °E. An enhancement of ΔS_2 takes place in the whole meridian from the SSW onset to ~55 days after the SSW onset except latitudes larger than 50 °S in the southern hemisphere. The prominent enhancement ranges from -50 °S to 40 °N, respectively. The striking positive ΔS_2 starts to appear at about -10 days before the SSW onset, reaches maximum at ~8 days and ends at ~50 days after the SSW onset at both EIA regions. Note that ΔS_2 has another peak at ~25 days at the northern EIA. At ~5 °N and ~30 °S, ΔS_2 starts to increase at ~10 days before SSW onset, reaches to its first peak of ~1.9 TECU in the period of 3 to 9 days and the second peak at ~25 days after SSW onset.

https://doi.org/10.5194/egusphere-2024-3177
Preprint. Discussion started: 28 October 2024

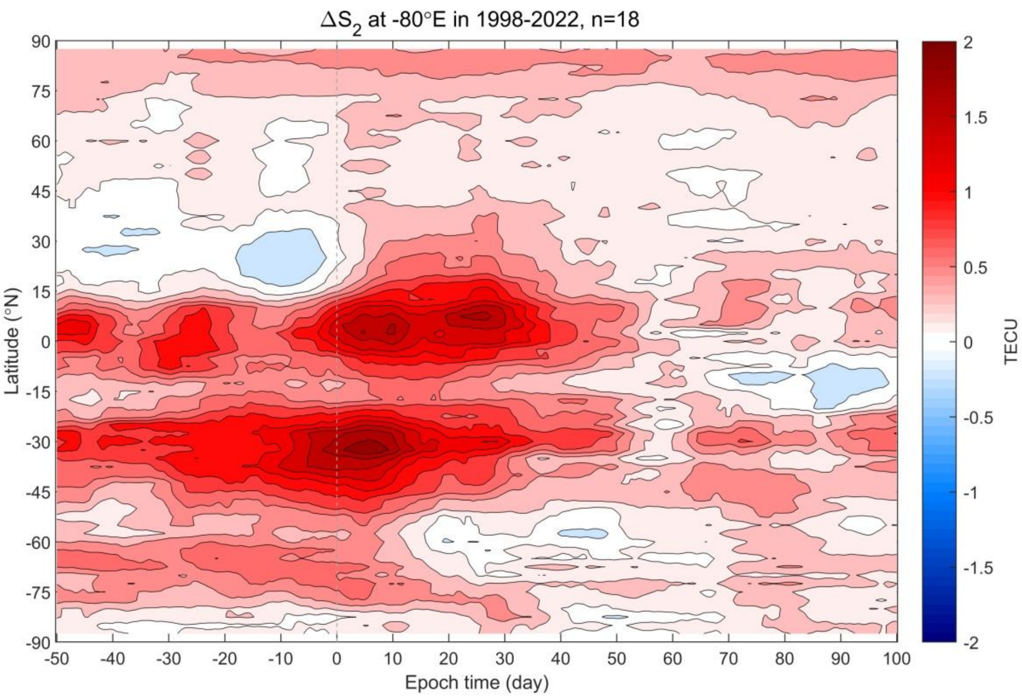

Figure 7. Time variation of meridian ΔS_2 at -80 °E, which is smoothed as a 14 d moving average. The vertical grey line marks the SSW onset day.

Figure 8 plots the temporal variation of ΔS_1 at the latitude of 20 °N, which is smoothed as a 14 d moving average. The ΔS_1 is generally enhanced from 0 to 50 days after the SSW onset for all longitudes except ~25 W where ΔS_1 starts to decrease from ~30 days after the SSW onset. ΔS_1 shows a maximum of ~1.3 TECU around 20-30 days after the SSW onset. It is notable that ΔS_1 increases earlier in the South America sector.

https://doi.org/10.5194/egusphere-2024-3177
Preprint. Discussion started: 28 October 2024

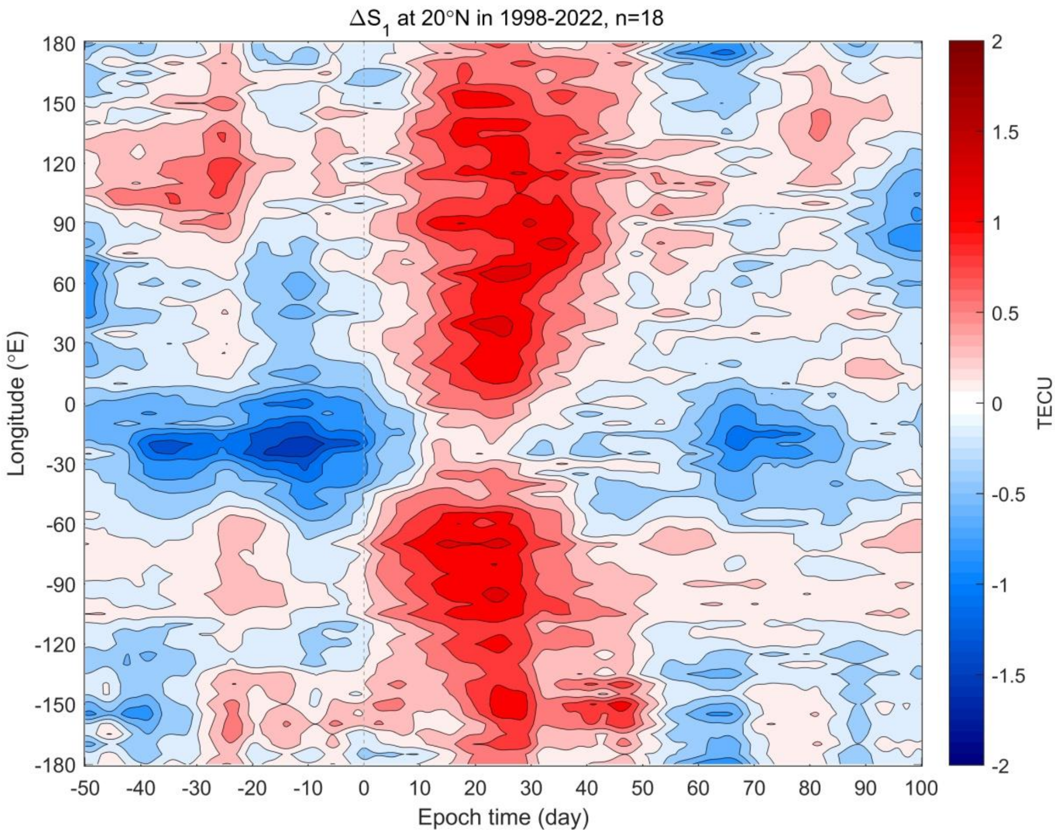

Figure 8. Time variation of zonal DeltaS1 at 20 °N, which is smoothed as a 14 d moving average. The vertical grey line marks the SSW onset day.

The temporal variation of zonal ΔS_2 at 22.5 °N is shown in figure 9, which is smoothed as a 14 d moving average. ΔS_2 is basically enhanced synchronously although the values of ΔS_2 are different at different longitudes. At two areas of 45 to 210 °E and -10 to -40 °E, ΔS_2 is generally positive. ΔS_2 starts to increase from -20 days which has a higher rate since a few days before the SSW onset. It reaches a maximum of ~1.5 TECU at ~8 days after the SSW onset. While ΔS_2 between 45-135 °N returns to the SSW onset level at ~45 days, ΔS_2 at the other area decreases to the SSW onset level at ~30 days. At

https://doi.org/10.5194/egusphere-2024-3177
Preprint. Discussion started: 28 October 2024

areas of -150 to -40 °E and -10 to 45 °E, ΔS_2 is at a level of ~0, and starts to increase at the SSW onset, reaches a maximum at ~10 days and decrease to a low level at ~30 days after the SSW onset.

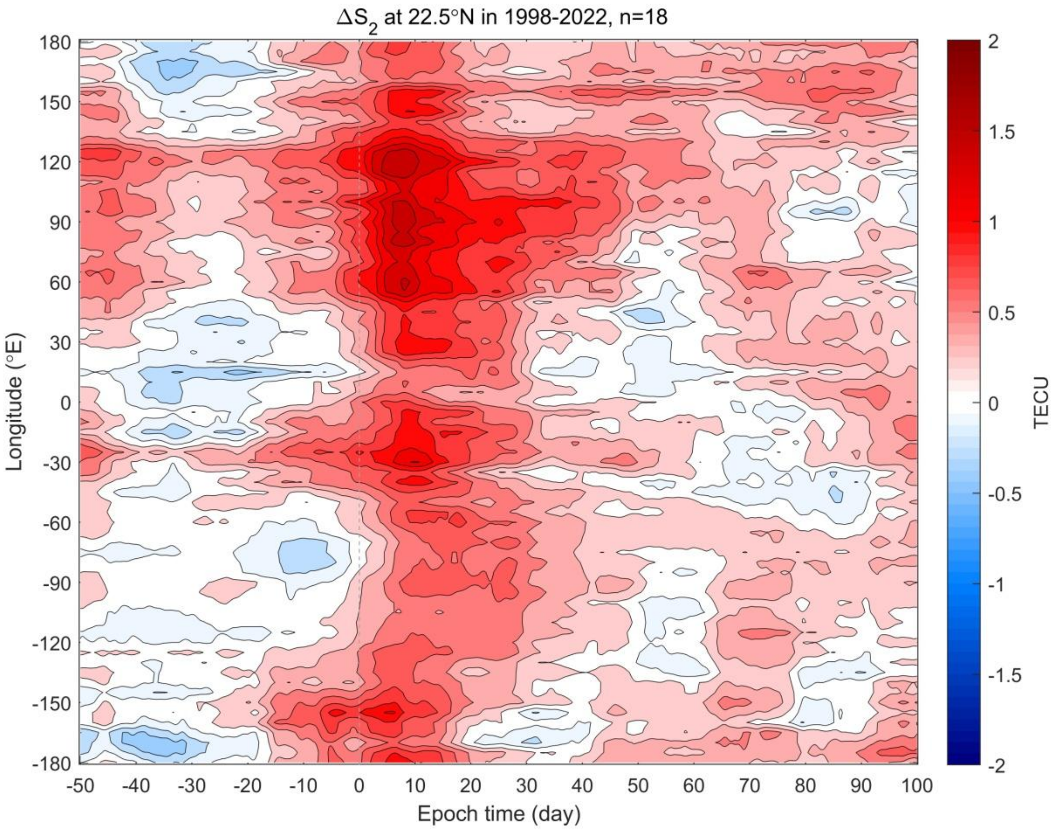

Figure 9. Time variation of zonal DeltaS2 at 22.5 °N, which is smoothed as a 14 d moving average. The vertical grey line marks the SSW onset day.

4 Discussion

The driving factors of the ionosphere consist of solar and magnetospheric energies from above and the atmospheric force from below. For the attribution of ionospheric response to SSW, it is crucial to separate the atmospheric waves from effects

https://doi.org/10.5194/egusphere-2024-3177
Preprint. Discussion started: 28 October 2024

due to solar/magnetospheric variability and seasonal variation. The case study of the SSW on 25 February 1999 in figure 3 shows intensified diurnal/semidiurnal variations of the observed TEC at 30 °N after the SSW onset. The diurnal/semidiurnal components from modeled TEC manifest contribution from solar/magnetospheric energies and seasonal change. The comparison between the observation and model suggests a clear SSW effect on low latitude ionosphere which is in agreement with previous studies (Chau et al., 2012; Liu et al., 2019).

Since the ionosphere has local characteristics and each SSW event may have a different effect due to complicated solar-terrestrial condition, it is justifiable to perform composite analysis described in the above analysis method. The 18 SSW events happened from 1998 to 2022, which cover two solar activity cycles. The composite analysis with the solar and magnetospheric effects removed would provide unambiguous evaluation of the SSW effects on the global ionosphere.

The world maps of DeltaS1 in figure 4 and DeltaS2 in figure 5 reveal that the SSW effect is generally global as depicted by Pedatella et al., 2018. SSW-induced amplifications of diurnal/semidiurnal tides can be identified from low to high latitudes with the strongest at EIA crests along the magnetic equator. Amplifications in semidiurnal tides during SSW have been revealed in low-latitude ionosphere from both case and statistical studies (Chau et al., 2012; Goncharenko et al., 2021; Hocke et al., 2024a). Semidiurnal disturbances in mid-latitude ionosphere have been only observed at Asian and America Sectors in Northern hemisphere (Xiong et al., 2013; Chen et al., 2016; Goncharenko et al., 2013; Liu et al., 2019). Our observation not only confirms the previous results but also displays that the semidiurnal pattern in mid-latitude ionosphere during SSWs is a global phenomenon. It is stronger at the mid-latitude Southern hemisphere than the Northern hemisphere. Concerning the diurnal variability, enhancement was once identified at low-latitide and a mid-latitude cite of Mohe (53.5 °N, 122.3 °E) for the SSW event in 2018 (Liu et al., 2019). The facts that the diurnal cycle shows enhancement in a global scale

https://doi.org/10.5194/egusphere-2024-3177
Preprint. Discussion started: 28 October 2024

and that the enhancement at the mid-latitude is larger Northern hemisphere than the Southern hemisphere are also new findings. Longitudinal differences exist in both diurnal and semidiurnal tides. Weaker amplification is obvious in Atlantic, African and Indian Sectors. This is especially true for the diurnal tide in Southern hemisphere.

As for the temporal variation due to atmospheric force below, DeltaS1 at 22.5 °N starts to increase simultaneously on the day of SSW onset in figures 6 and 8. It reaches to the peak around 20-30 days after SSW onset. The positive effect lasts to ~50 days after SSW onset. DeltaS2 at -80 °E, as shown in figure 7, starts to increase simultaneously at ~10 days before SSW onset. It peaks at ~8 days and recovers at ~50 days after the SSW onset. At other longitudes in figure 9, the semidiurnal component starts to enhance at ~20 days before SSW onset, peaks at ~8 days after SSW onset. Note that the enhancement lasts generally to ~50 days after SSW onset while the prominent effect happens between 60 and 120 °E, the Asia region. The review by Goncharenko et al. (2021) has summarized that the main SSW effect is a distinct semidiurnal variation in thermospheric and ionospheric parameters that lasts for days up to 30–40 days. The results of the comprehensive composite analysis for 18 SSW events demonstrate that the enhancement of both diurnal and semidiurnal components last for ~50 days. While the semidiurnal enhancement starts earlier and peaks at ~8 days after SSW onset, the diurnal one starts on the SSW onset day and peaks around 20-30 days after SSW onset.

The SSW effects on the tidal ionospheric TEC variations are a global phenomenon, though there is no clear SSW effect on the ionospheric TEC in high-latitude. The complicated patterns of the SSW-induced tidal ionospheric TEC variations indicate multiple dynamical processes might be involved during SSWs. We speculate that the SSW related E-region dynamo is the main mechanism which is generally not strong enough to produce vertical plasma drifts in high-latitude.

5 Conclusions

We present the comprehensive composite analysis of the ionospheric tidal variability in association with 18 sudden stratospheric warming events by using the global total electron content data from 1998 to 2022. To extract TEC variations from effects of SSWs and atmospheric forcing below the ionosphere, we first model the TEC climatology due to solar activity, magnetospheric energy and seasonal change by neural network training for the observed time series of global TEC, then we remove the modelled TEC from the observed TEC. Our analysis reveals for the first time a globally SSW-induced enhancement in both semidiurnal and diurnal TEC variations. The semidiurnal TEC variation is the strongest at equatorial ionospheric anomaly (EIA) crests along the magnetic equator, which is in agreement with previous studies. At mid-latitude the semidiurnal variation is larger in the Southern hemisphere than the Northern hemisphere. Another finding of the paper is the diurnal TEC variation in low-latitude has a similar behaviour to the semidiurnal one. The diurnal TEC enhancement at the mid-latitude is larger in Northern hemisphere than the Southern hemisphere, contrary to the semidiurnal one. Clear SSW effects are not seen in the high latitude ionosphere. Both tidal TEC variations show longitudinal dependence with weaker amplification in Atlantic, African and Indian Sectors. This is especially true for the diurnal tide in Southern hemisphere. While the semidiurnal enhancement starts earlier and peaks at ~8 days after SSW onset, the diurnal one starts on the SSW onset day and peaks around 20-30 days after SSW onset. Both semidiurnal and diurnal enhancements last to about 50 days after SSW onset.

Our analysis indicates that multiple dynamical processes might be involved during SSWs from the hemispheric asymmetry and longitudinal differences in diurnal/semidiurnal variations of TEC. It is likely that the SSW related E-region dynamo is the main mechanism which is generally not strong enough to produce discernible TEC variations in high-latitude ionosphere. The ML-TEC model can separate the SSW effects on the ionosphere from dependences on solar/geomagnetic activities and

https://doi.org/10.5194/egusphere-2024-3177
Preprint. Discussion started: 28 October 2024

season. This is a new analysis method which is important for SSW analysis since the tidal amplitudes in the upper atmosphere have a strong seasonal dependence. The regular, seasonal enhancement of tidal amplitudes in northern hemispheric winter can be wrongly attributed to SSWs since SSWs mainly happen in northern hemispheric winter. Our ML-TEC model avoids such a false attribution.

Code availability. MATLAB codes can be provided upon request.

Data availability. The TEC data are a product of IGS, which are freely available at Crustal Dynamics Data Information System, NASA's archive of space geodesy data https://cddis.nasa.gov/. The Data about solar and geomagnetic activity was obtained from the GSFC/SPDF OMNIWeb interface at https://omniweb.gsfc.nasa.gov (accessed on 2023).

https://doi.org/10.5194/egusphere-2024-3177
Preprint. Discussion started: 28 October 2024

Author contributions. The Concept of the study: KH and GM. Data analysis: GM and KH. Writing: GM. Corrections and discussion of the paper: KH and GM.

Competing interests. The contact author has declared that none of the authors has any competing interests.

Acknowledgements. We thank the WDC for Ionosphere and Space Weather (National Institute of Information and Communications Technology, Tokyo) for providing the long-term foF2 series for Okinawa and for the operation of the ionosonde. We also thank the Meridian Project for providing the ionosonde data for Wuhan. The reviewers are thanked for their valuable comments and improvements.

Financial support. This research was funded by the Swiss National Science Foundation, grant number IZSEZ0-224443; the National Natural Science Foundation of China (Nos. 12073049 and 12273062), and the CAS-JSPS Joint Research Project (178GJHZ2023180MI).

References

Chau, J. L. , Goncharenko, L. P. , Fejer, B. G. , & Liu, H. L.: Equatorial and low latitude ionospheric effects during sudden stratospheric warming events, Space Science Reviews, 168(1-4), 385-417, 2012.

Chen, G., Wu, C., Zhang, S., Ning, B., Huang, X., et al.: Midlatitude ionospheric responses to the 2013 SSW under high solar activity, Journal of Geophysical Research: Space Physics, 121, 790–803, doi:10.1002/2015JA021980, 2016.

Chernigovskaya, M.A., Shpynev, B. G., Ratovsky, K. G., Belinskaya, A. Yu., Stepanov, A. E., & Bychkov, V. V.: Ionospheric response to winter stratosphere/lower mesosphere jet stream in the Northern Hemisphere as derived from vertical radio sounding data. Journal of Atmospheric and Solar-Terrestrial Physics, 180, 126–136. doi:10.1016/j.jastp.2017.08.033, 2018.

Fuller-Rowell, T., Wu, F., Akmaev, R., Fang, T.-W., & Araujo-Pradere, E.: A whole atmosphere model simulation of the impact of a sudden stratospheric warming on thermosphere dynamics and electrodynamics, Journal of Geophysical Research, 115, A00G08. doi: 10.1029/2010JA015524, 2010.

Goncharenko, L. P., Hsu, V. W., Brum, C. G. M., Zhang, S.-R., & Fentzke, J. T.: Wave signatures in the midlatitude ionosphere during a sudden stratospheric warming of January 2010, Journal of Geophysical Research: Space Physics, 118(1), 472–487, doi:10.1029/2012JA018251, 2013.

Goncharenko, L. P., Harvey, V. L., Liu, H., & Pedatella, N. M.: Sudden Stratospheric Warming Impacts on the Ionosphere–Thermosphere System: A Review of Recent Progress, Space Physics and Aeronomy Collection Volume 3: Ionosphere Dynamics and Applications, Geophysical Monograph 260, First Edition, Edited by Chaosong Huang and Gang Lu. © 2021 American Geophysical Union, Published 2021 by John Wiley & Sons, Inc, 2021.

Hagan, M. T. and Menhaj M. B.: Training feedforward networks with the Marquardt algorithm, IEEE Transactions on Neural Networks, vol. 5, 989-993, doi: 10.1109/72.329697, 1994.

Hernández‐Pajares, M., Juan, J. M., Sanz, J., Orus, R., Garcia‐Rigo, A., Feltens, J., et al.: The IGS VTEC maps: A reliable source of ionospheric information since 1998. Journal of Geodesy, 83(3), 263–275. https://doi.org/10.1007/s00190‐008‐0266‐1, 2009.

Hocke, K., Wang, W., Ma, G.: Influences of sudden stratospheric warmings on the ionosphere above Okinawa. Atmospheric Chemistry and Physics, 24(10), 5837–5846. https://doi.org/10.5194/acp‐24‐5837‐2024, 2024a.

Hocke, K., Wang, W., Cahyadi, M. N., Ma, G.: Quasi‐diurnal lunar tide O1 in ionospheric total electron content at solar minimum. Journal of Geophysical Research: Space Physics, 129, e2024JA032834. https://doi.org/10.1029/2024JA032834, 2024b.

Jin, H., Miyoshi, Y., Pancheva, D., Mukhtarov, P., Fujiwara, H., Shinagawa, H.: Response of migrating tides to the stratospheric sudden warming in 2009 and their effects on the ionosphere studied by a whole atmosphere-ionosphere model GAIA with COSMIC and TIMED/SABER observations, Journal of Geophysical Research, 117, A10323, doi:10.1029/2012JA017650, 2012.

Liu, G., Huang, W., Shen, H., Aa, E., Li, M., Liu, S., Luo, B.: Ionospheric response to the 2018 sudden stratospheric warming event at middle‐ and low‐latitude stations over China sector. Space Weather, 17, 1230–1240. https://doi.org/10.1029/2019SW002160, 2019.

Pedatella, N. M., and Liu, H.-L.: The influence of atmospheric tide and planetary wave variability during sudden stratosphere warmings on the low latitude ionosphere. Journal of Geophysical Research, 118, 5333–5347. doi:10.1002/jgra.50492, 2013.

https://doi.org/10.5194/egusphere-2024-3177
Preprint. Discussion started: 28 October 2024

Pedatella, N. M., Liu H.-L., Sassi, F., Lei, J., Chau, J. L., Zhang X.: Ionosphere variability during the 2009 SSW: Influence of the lunar semidiurnal tide and mechanisms producing electron density variability, J. Geophys. Res. Space Physics, 119, 3828–3843, doi:10.1002/2014JA019849, 2014.

Pedatella, N.M., Chau, J.L., Schmidt, H., Goncharenko, L.P., Stolle, C., Hocke, K., Harvey, V., Funke, B., Siddiqui, T.A.: How sudden stratospheric warmings affect the whole atmosphere, EOS, Transactions AGU 2018, 99, 35-38. https://doi.org/10.1029/2018EO092441, 2018.

Xiong, J., Wan, W., Ding, F., Liu, L., Ning, B., Niu, X.: Coupling between mesosphere and ionosphere over Beijing through semidiurnal tides during the 2009 sudden stratospheric warming, Journal of Geophysical Research: Space Physics, 118(5), 2511–2521, 2013.